Towards a Cosmological Hubble Diagram for Type II-P Supernovae

Peter Nugent[1], Mark Sullivan[2], Richard Ellis[3], Avishay Gal-Yam[3,4], Douglas C. Leonard[3,5], D. Andrew Howell[2], Pierre Astier[6], Raymond G. Carlberg[2], Alex Conley[2], Sebastien Fabbro[7], Dominique Fouchez[8], James D. Neill[9], Reynald Pain[6], Kathy Perrett[2], Chris J. Pritchet[9] and Nicolas Regnault[6]

penugent@LBL.gov

ABSTRACT

We present the first high-redshift Hubble diagram for Type II-P supernovae (SNe II-P) based upon five events at redshift up to $z \sim 0.3$. This diagram was constructed using photometry from the Canada-France-Hawaii Telescope Supernova Legacy Survey and absorption line spectroscopy from the Keck observatory. The method used to measure distances to these supernovae is based on recent work by Hamuy & Pinto (2002) and exploits a correlation between the absolute brightness of SNe II-P and the expansion velocities derived from the minimum of the Fe II 5169Å P-Cygni feature observed during the plateau phases. We present three refinements to this method which significantly improve the practicality of measuring the distances of SNe II-P at cosmologically interesting redshifts. These are an extinction correction measurement based on the $V - I$ colors at day 50, a cross-correlation measurement for the expansion velocity and the ability to extrapolate such velocities accurately over almost the entire plateau phase. We

---

[1]Lawrence Berkeley National Laboratory, 1 Cyclotron Road, Berkeley, CA 94720, USA

[2]University of Toronto, 60 St. George Street, Toronto, ON M5S 3H8, Canada

[3]California Institute of Technology, E. California Blvd, Pasadena CA 91125, USA

[4]Hubble Postdoctoral Fellow

[5]NSF Astronomy and Astrophysics Postdoctoral Fellow

[6]LPNHE, CNRS-IN2P3 and University of Paris VI & VII, 75005 Paris, France

[7]CENTRA - Centro Multidisciplinar de Astrofísica, IST, Avenida Rovisco Pais, 1049 Lisbon, Portugal

[8]CPPM, CNRS-IN2P3 and University Aix Marseille II, Case 907, 13288 Marseille Cedex 9, France

[9]Department of Physics and Astronomy, University of Victoria, PO Box 3055, Victoria, BC V8W 3P6, Canada

apply this revised method to our dataset of high-redshift SNe II-P and find that the resulting Hubble diagram has a scatter of only 0.26 magnitudes, thus demonstrating the feasibility of measuring the expansion history, with present facilities, using a method independent of that based upon supernovae of Type Ia.

Subject headings: supernovae – cosmology – Type II-P supernovae

1. Introduction

The discovery of a cosmic acceleration based on the analysis of the Hubble diagram of Type Ia supernovae (SNe Ia; Riess et al. 1998; Perlmutter et al. 1999) has far-reaching implications for our understanding of the Universe. While indirect evidence for the acceleration can be deduced from a combination of studies of the cosmic microwave background and large scale structure (Efstathiou et al. 2002; Bennett et al. 2003; Eisenstein et al. 2005) distance measurements to supernovae provide a valuable direct and model independent tracer of the evolution of the expansion scale factor necessary to constrain the nature of the proposed dark energy. The mystery of dark energy lies at the crossroads of astronomy and fundamental physics: the former is tasked with measuring its properties and the latter with explaining its origin.

Systematic uncertainties (rather than statistical errors) may soon limit SN Ia measurements of the expansion rate at $z \sim 0.5$ (see Knop et al. 2003; Astier et al. 2005, for recent analyses). A largely unexplored source of potential bias is evolution in the progenitor properties and/or the SN explosion. While several programs are underway to measure, test, and constrain SN Ia systematics (Sullivan et al. 2005; Ellis et al. 2006), it is highly desirable to consider independent tests of the cosmology where both the underlying physics and susceptibility to bias and evolution are different.

As cosmological probes, SNe II have lagged behind their brighter and better calibrated cousins, SNe Ia, but their potential has improved significantly as a result of several recent studies. Baron et al. (2004); Baron et al. (2003); Mitchell et al. (2002), and two doctoral theses (Hamuy 2002; Leonard 2000), have utilized new samples of SNe II and demonstrated that a subset, the plateau SNe II-P, are particularly promising as distance indicators. From an astrophysical standpoint, SNe II-P hold three advantages over SNe Ia as cosmological probes: (1) Their progenitor stars are well understood, (Heger et al. 2003; Li et al. 2005; Smartt et al. 2003), (2) the physics of their atmospheres, dominated by hydrogen, is much simpler to understand and model (Baron et al. 2004), and (3) while fainter, they are more abundant per unit volume (Mannucci et al. 2005; Cappellaro et al. 2005). The two main disadvantages are that they are on average 1.2 magnitudes fainter in the optical than SNe Ia and that all distance measurements currently based on SNe II-P require a reasonable-quality spectrum of the event.

Unlike the other members of the core-collapse supernova family, SNe II-P maintain a massive hydrogen envelope prior to explosion. From analyses of their optical light curves and spectra (e.g., Chugai 1994), they evidently suffer little subsequent interaction with the surrounding medium – they are the result of the putative red supergiant exploding into a near-vacuum. Recent results from spectropolarimetric studies also suggest that, at least during the plateau epoch, the ejecta and electron-scattering photosphere are quite spherical (see Leonard & Filippenko (2005) and references therein).

For SNe II-P, distance measurements from the spectral expanding atmosphere method (SEAM; see Baron et al. 2004), the descendent of the traditional expanding photosphere method (EPM; see Kirshner & Kwan 1974; Schmidt 1993), can be replaced by a more practical empirical method which requires less input data, as developed in Hamuy & Pinto (2002); Hamuy (2003) (hereafter HP02 and H03 respectively). The approach advocated by HP02 is a particularly significant development since it is motivated by sound physical principles. In more luminous supernovae, the hydrogen recombination front is maintained at higher velocities, pushing the photosphere farther out in radius. When a SN II-P is on the plateau phase, a period which lasts for around 100 days, a strong correlation is expected and observed between the velocity of the weak Fe II lines near 5000 Å (which suitably track the electron-scattering photosphere) and the luminosity.

Calibration of these standardized candles requires line of sight extinction corrections, which can be determined in one of two ways. When the supernova leaves the plateau phase, the photospheric temperature should be close to that of recombination, and thus the observed color at this point will provide a reddening estimate. Alternatively, for well-studied SNe II-P, one can employ detailed modeling of a series of high signal-to-noise spectra to determine the extinction. Here, deviations between the line profiles of selected absorption features and those expected given the observed spectral energy distribution (SED) can be used to estimate selective extinction. Application of these techniques to 24 SNe II-P in the Hubble flow (Fig. 1 of H03) yields a I-band Hubble diagram with a scatter of only 0.29 magnitudes, corresponding to a precision of 15% in distance.

The present paper is concerned with extending the HP02 method so that it can be used at cosmological distances. Although economical compared to the SEAM/EPM methods in terms of input data, the HP02 method is still poorly suited as a basis for verifying the cosmic acceleration due to the difficult demands on spectroscopy and the photometric measurements necessary for an extinction correction at high-redshift. Our discussion is timely because of the feasibility of locating distant SNe II-P from comprehensive 'rolling searches' such as the Canada-France-Hawaii Telescope SN Legacy Survey (SNLS; Astier et al. 2005). Such surveys can generate SNe II-P with $0.1 < z < 0.4$ continuously with tight constraints on their explosion dates and excellent photometric coverage, making pre-scheduled spectroscopic campaigns to measure the expansion rate during the plateau phase a practical proposition.

A plan of the paper follows. In §2 we introduce an enhanced local dataset suitable for exploring the potential of an improved method and detail the difficulties we need to overcome to use the HP02 method at intermediate redshifts. We then introduce two extensions to the method and show, via our dataset, that we can retain the precision with indicators of velocity and extinction more suited to high redshift datasets. In §3, we present the first observations of high-redshift SNe II-P obtained via SNLS and construct a Hubble diagram from these supernovae which demonstrate the feasibility of locating and studying high redshift SNe II-P for verifying the cosmic acceleration. We summarize our conclusions in §4.

2. Improving the HP02 Method

The drawbacks of the method introduced by HP02 for studies of cosmologically distant SNe II-P are two-fold.

Foremost, the extinction correction cannot be measured using colors determined at the end of the plateau phase since its precise timing would require continuous monitoring, which is impractical for faint supernovae, and at intermediate redshift, SNe II-P discovered prior to the time they explode will typically be too close to the sun at this stage in their evolution. Moreover, corrections for extinction based on this method in H03 often produced negative results. Likewise, the signal/noise of plateau spectra will generally not be adequate for detailed spectrum synthesis modeling of various line profiles in order to determine the intrinsic SED. We thus seek a more appropriate way to estimate the line of sight extinction.

Secondly, it is a challenge at moderate redshift to secure accurate measures of the weak diagnostic Fe II 5169Å line used to measure the photospheric expansion during the plateau phase, even with the largest ground-based telescopes. In particular, as diagnostic lines in this region of the spectrum are redshifted into the OH forest beyond $z \simeq 0.5$, so it becomes advantageous to explore alternatives should the Fe II 5169Å line profile be polluted by a sky feature. We therefore wish to explore the practicality of alternative, stronger lines to measure the photospheric expansion.

To explore the possibilities, we have constructed a sample of nearby SNe II-P which includes all of those in H03 for which there is both V- and I-band data. We also include

SN 2004dh, a SN discovered by LOSS (Moore & Li 2004) and followed as part of the Caltech Core-Collapse Program (CCCP; see Gal-Yam et al. 2004; Gal-Yam et al. 2006a), which leads to a total of 19 SNe II-P. We have updated the distances to two supernovae presented in H03. In the case of SN 1999em we use the *HST*-determined Cepheid distance to the host (Leonard et al. 2003). For SN 1999gi we use the improved distance derived via a variety of methods as discussed in Leonard et al. (2002). These changes have very little effect on the overall fit as both galaxies are nearby with large uncertainties in their relative distances. We have also removed all of the extinction corrections applied in H03.

We now turn to two improvements necessary to enable us to use SNe II-P as distance indicators at moderate redshift.

2.1. Incorporating $V-I$ Colors

The first modification of the HP02 method we have explored makes use of the restframe $V-I$ color during the plateau phase at day 50 to perform an extinction correction rather than relying on colors at the end of the plateau phase or on detailed modeling, as in H02. Our goal is to explore empirically the extent to which we can retain a tight Fe II velocity-luminosity relation using the observed $V-I$ color at this epoch.

If we fit for the velocity and luminosity using plateau-phase data, interpolated to day 50, we find:

$$M_I = -\alpha\, log_{10}\,(V_{FeII}/5000) - 1.36[(V-I)-(V-I)_0] + M_{I_0} \tag{1}$$

Here, as in H03, we have adopted the relative SBF distance scale (Tonry et al. 2000). The resultant fit to the data yields $\alpha = 6.69 \pm 0.50$ and $M_{I_0} = -17.49 \pm 0.08$ ($H_0 = 70$ kms sec^{-1} Mpc^{-1}) for a $(V-I)_0 = 0.53$. In this fit we have employed the standard relationship between the $V-I$ colors for a dust law with $R_V = 3.1$ for a SN II-P at day 50 ($A_I = 1.36 * E_{V-I}$). As is done in the SN Ia studies (Guy et al. 2005) for the color stretch-relationship, we have adopted a ridge-line, unextinguished $(V-I)_0$ color for SN II-P of 0.53 magnitudes. Under the assumption that the extinction laws are similar from galaxy to galaxy, the exact choice is irrelevant since this term and the M_{I_0} term are degenerate for the purpose of using these objects as cosmological probes. Using this technique we can produce a Hubble diagram in restframe I-band with a scatter of only 0.28 magnitudes (Figure 1) for those SNe II-P in the Hubble flow ($cz > 3000$ km/s), similar to that found in H03. The scatter for all SN II-P is reduced from 1.11 to 0.52 magnitudes. Crucially, we find there is no advantage in using reddening estimators based on late-time color measures or on detailed modeling of the spectroscopic data.

To address the robustness of this simple approach, we investigated solutions where we permit an additional parameter based upon a possible relationship between the Fe II velocity and the dereddened $V-I$ color. One could easily envision a correlation that brighter SN II-P were faster *and* bluer. However, the correlation we find is weak and lacks any statistical significance.

We note that for $\alpha \neq 5.0$ ($\alpha = 5$ implies that the luminosity follows the square of the radius only), there presumably does exist an additional correlation between the effective temperature and density of the expanding photosphere and its radius, so conceivably there is some scope for further improvement in defining Eq. 1. Future work, such as the ongoing research by the CCCP and the Carnegie Supernova Project (CSP) (Freedman 2005), will be helpful in clarifying the possibilities and allow us to address the strongly correlated issues of extinction corrections and velocity-dependent colors.

2.2. Using Alternative Lines to Diagnose the Photospheric Expansion

We now explore whether alternative absorption lines can be used in addition to Fe II 5169Å as diagnostics of the photospheric expansion velocity. Over the wavelength range 4500-5500Å there exist several Fe II lines (the strongest of which are at 4924, 5018 and 5169Å). Moreover, often the $H\beta$ 4861Å absorption line is prominent. Depending on the supernova and its phase, the relative strengths of these lines can vary considerably (see Figure 2). In general, at earlier epochs $H\beta$ tends to dominate while a later epochs the Fe II lines are the dominant absorption features over this wavelength range. Accordingly, if at higher redshift we are able to compare to any or all of these lines we can minimize the effects of the interference with OH night sky features and any underlying host galaxy contamination.

In order to explore possible systematic effects arising from the use of using different absorption lines as measures of the expansion, we will first examine trends in local data. To do this we assembled a library of SNe II-P spectra based on data from the SUSPECT database[10] for: SNe 1969L, 1988A, 1988H, 1993W, 1999gi and 1999em(Benetti 1991; Turatto et al. 1993; Leonard et al. 2002, 2003; Hamuy et al. 2001; Baron et al. 2003) as well as data from the first year of the CCCP: SNe 2004A, 2004T, 2004dh, 2004du, 2004em and 2004et

[10]see: http://bruford.nhn.ou.edu/˜suspect/index1.html

(Gal-Yam et al. 2006b). A particularly important question is whether it is safe to use $H\beta$ as a diagnostic rather than the Fe II lines, given the former is often quite strong. In what follows, we have divided the local dataset into two categories: those dominated by the $H\beta$ feature and those dominated by the Fe II features (defined according to whether the equivalent width of $H\beta$ is respectively greater than or less than that of the sum of the Fe II features). The motivation here is two-fold. Firstly, unlike $H\beta$, in the case of the Fe II-dominated spectra, the weak lines form at the same location in the atmosphere near the electron scattering photosphere. Thus we might expect any (or all) of them to be acceptable for measuring the velocity. Secondly, as we will later test a novel cross-correlation method across this wavelength range, it is very helpful to understand possible systematic velocity differences between Hβ and the Fe II lines. For both Fe II 5169Å and Hβ, we measured absorption velocities using a routine in which we first subtract the continuum, take the wavelength derivative and then fit for the wavelength where this derivative changes sign.

Figure 3 shows that, in the $H\beta$-dominated spectra, the velocity of $H\beta$ is significantly higher than that of Fe II 5169Å with the trend that the ratio of $H\beta$ to Fe II drops towards unity only at very high velocities. Clearly simply replacing Fe II absorption velocities with measures of Hβ would lead to erroneous results. However, if we fit this ratio in two sections, a constant for velocities below 6000 km/s ($ratio = 1.395$) and a linear decline for higher velocities ($ratio = 1.395 - 6.489 * 10^{-5}(V(H\beta) - 6000)$), the dispersion about this relationship (± 0.054) translates to an uncertainty in estimating the Fe II velocity from $H\beta$ measures of only $\sim$300 km/s.

Of course, before accepting such an empirical correction, it is important to understand the trend physically. To accomplish this, we examined spectrum synthesis fits to model SNe II-P discussed by Baron et al. (2004). The predicted trend is qualitatively similar in form to that observed and, in particular, reproduces the decline in the ratio observed at higher velocities. The model spectra with higher effective temperatures were in general from earlier epochs with higher velocities, while the cooler ones were later with lower velocities. The optical depth of $H\beta$ is strongly tied to the level of ionization of hydrogen. Thus as the temperature drops, the velocities fall, less hydrogen is ionized and the optical depth of $H\beta$ increases significantly compared to the weak Fe II lines. This in turn increases the ratio.

In order to maximize the information content in either the series of weak Fe II lines or in the $H\beta$-dominated spectra, we then examined a cross-correlation analysis across the wavelength range 4500-5500Å . In the Fe II dominated spectra we simply compared the measured Fe II 5169Å velocities to those obtained in the cross-correlation analysis. For the $H\beta$ dominated spectra we compare the measured $H\beta$ velocities and then reduced these to equivalent Fe II 5169Å velocities using the fit to the ratio defined above. In performing crosscorrelations, all spectra are continuum subtracted and analyzed in log-wavelength space in the manner described by Tonry & Davis (1979).

A measure of the potential bias and systematic uncertainty arising in the cross-correlation method can be obtained by considering the distribution of velocity differences obtained by multiple template comparisons within our local dataset (Figure 4). Each local supernova, when compared to the average of the cross-correlation calculated velocities, shows differences of typically $<$150 km/s. This is a measure of *template mismatch* for the local sample in the wavelength region sample, i.e. in individual SNe II-P, the strongest features present can form at slightly different velocities than Fe II 5169Å in addition to measurement uncertainties for the minimum of that line in our spectral library. This bias is recorded for each of our template spectra and subtracted off when used in the cross-correlation measurement. The resultant measured dispersion in comparing one of our template spectra to the rest in their respective sets is 160 km/s for $H\beta$-dominated spectra and 110 km/s for the Fe II-dominated spectra

Of course these tests calibrate systematic uncertainties that are dominant only for low redshift SNe IIP. At high redshift we can expect an additional component from the lower signal to noise implicit in the fainter sources. To estimate how effective this method will be at intermediate redshift, where our signal-to-noise is typically between 8-20 per 2Å over the relevant wavelength range, we performed a Monte Carlo equivalent of the above test by degrading the signal-to-noise of the nearby spectra to 7 per 2Å. The resulting dispersion for individual measurements increased by only 15 km s^{-1}, clearly showing that the cross-correlation method is sufficiently accurate for our purpose.

The final problem we must overcome in facilitating a cosmological application of SNe II-P concerns the fact that it is impractical to schedule, in advance, a spectroscopic night at day 50 for each supernova of interest. Thus we need to explore how well we can extrapolate the velocity from a given epoch to day 50. While published data with the run of velocity with time is limited, that available to us indicates that the time dependence of the Fe II 5169Å velocity can be well represented by a power law of the form:

$$V(50) = V(t) * (t/50)^{0.464\pm0.017} \tag{2}$$

(see Figure 5). Extrapolation for epochs between 9 and 75 days to day 50 can be made quite reliably adding an uncertainty of $<$175 km/s. Adding the various uncertainties in quadrature indicates expansion velocities of distant SNe II-P should be typically accurate to $\simeq$220 km/s.

3. A Cosmological Hubble Diagram Based on a Sample of High Redshift SNe II-P

In the previous section, we have shown that extinction corrections using $V - I$ colors during the plateau phase at day 50 and concurrent expansion velocities determined using a variety of prominent absorption lines can be used to generalize and extend the important distance determination method initially proposed by HP02. As SNe II-P are now being found to redshifts $z \simeq 0.4$ in rolling searches such as the SNLS (Sullivan et al. 2005), we can now apply our method to these distant supernovae to independently verify the cosmic acceleration.

Starting in 2003, we began using the Low Resolution Imaging Spectrometer [LRIS; Oke et al. (1995)], a double-arm spectrograph mounted on the 10-m Keck I telescope, to observe SNLS-discovered supernovae. Although our primary program initially targeted SNe Ia (Ellis et al. 2006), during the first two years we also successfully studied five moderate-redshift ($0.1 < z < 0.3$) SNe II-P, identified from the SNLS rolling search via their light curves. These events were typically observed five times per lunation in $g'r'i'z'$ (Astier et al. 2005) with coverage starting before explosion and extending throughout the plateau phase (see Figures 6–10).

We measure $g'r'i'z'$ fluxes of the SNLS supernovae using a PSF-fitting technique. The first step is to perform a photometric alignment of each supernova observation to secondary standards within each field using a multiplicative scaling factor, and assign an astrometric solution using custom-built astrometric reference catalogs. Deep "references" are constructed to contain no supernova light, and are resampled to the pixel co-ordinate system of each observation. The references are then PSF-matched and subtracted from each individual observation, leaving a difference image containing only supernova photons. The fluxes are then estimated by fitting a PSF profile measured from stars in the un-subtracted image at the known position of the supernova, with the weighting in each pixel equal to $1/\sigma^2$, where σ is calculated from the background sky noise and the Poisson noise from the supernova and host photons. An average flux measurement on each night of observation is made using a sigma-clipped weighted average of the individual data frames.

Keck spectra were taken on the plateau over a range in time of $15 < t < 75$ restframe days (see Figure 11). The Keck-LRIS observing configuration used the 560 dichroic, with the 600l/mm grism blazed at 4000Å on the blue side, and the 400l/mm grating blazed at 8500Å on the red side. The grating central wavelength was adjusted to ensure a complete wavelength coverage from 3500Å to 9200Å. Depending on seeing conditions, either a $1''$ or $0.7''$ slit was used, and the supernova was dithered between each 1800s exposure by 3-5$''$. Typical total exposure times were 2-3 hours, and all data were taken at the parallactic angle. All spectroscopic data was processed using a pipeline developed by one of us (MS), which performs basic bias subtraction and flat-fielding, as well as a fringe subtraction on the red side using a fringe frame constructed from an entire night's data. Each exposure was extracted separately on the red and blue sides, wavelength and flux-calibrated, corrected for atmospheric extinction, and optimally combined with the other exposures to form one continuous spectrum.

To calculate the restframe $V-I$ colors during the plateau phase, we first made an estimate of the explosion date of the supernova conservatively based on the midpoint between the last non-detection and the first detection of the supernova in any filter during the rolling search. We then interpolated the $g'r'i'z'$ colors at day $50(1+z)$. These colors were used to "warp" a day 50 template SN II-P spectrum, redshifted appropriately, following the protocol described in Nugent et al. (2002) with the exception that here we use spline fits to the underlying colors to adjust the template rather than a reddening law. This spectrum was then de-redshifted and the restframe $V-I$ color of the supernova was calculated.

The Fe II velocities were measured via the cross-correlation technique introduced in § 2.2, extrapolated to restframe day 50 using Eq. 2. In determining the velocity and its uncertainty from the full range of local templates, we adopted the *Median Absolute Deviation* method, which provides a particularly robust measure of the dispersion when there are a few significant outliers. The distribution of cross-correlation velocities is calculated using all local templates and the median of the distribution estimated. The absolute modulus of the deviation from the median velocity is calculated and that distribution is medianed and 3σ clipped. We then take the mean of the remaining velocities and the rms about this mean as our velocity and uncertainty. Typically, this procedure reduced the comparison library by <25%. The correlations and resulting best fits can be seen in Figure 12 and are listed in Table 1 and 2.

Appropriately dealing with uncertainties in the above measurements, and evaluating their implications on the inferred distances is an important aspect of our analysis. An uncertainty in the explosion date will propagate to one in the distance determination. On the one hand the expansion velocity will decline (implying a lower luminosity) as the explosion date is moved forward, whereas the SN will get redder with time on the plateau, implying more extinction (and a more luminous event). To quantify such biases, we devised a Monte Carlo simulation incorporating these uncertainties. The results in Table 3 summarize both the measurements and their uncertainties as a result of these simulations. To illustrate the potential value of our Hubble diagram, we performed a cosmological fit using both these and and the low-redshift supernova (Table 4) under the assumption of the flat cosmological model found in Astier et al. (2005).

The values of the fitting parameters in this joint fit of both the high and low redshift SNe II-P changed to $\alpha = 5.81$ and $M_{I_0} = 17.52$. This value of α is lower by 1.5-σ compared to the fit for only the low-redshift SNe II-P, see Figure 14. The observed scatter was 0.26 magnitudes for all supernovae in the Hubble flow. The Hubble diagram is presented in Figure 13. The reduced χ^2 is 1.8 which implies an intrinsic dispersion of 0.12 magnitudes, though this number is quite tentative due to the low number statistics involved in this analysis.

Two of the problems facing this dataset of SNe II-P are the data-analysis inconsistencies between the low and high-redshift data and small number statistics. The low redshift data assembled in H03 measured and then extrapolated/interpolated the velocities in a manner different than the one presented here (though for high-quality data with strong time constraints, there should be little to no difference between the techniques). In addition, a large fraction of the data in H03 involves SNe II-P not in the Hubble flow. Our five additional high-redshift supernovae, and one low-redshift SN II-P, increased this pool of data from 8 to 14. To address these issues and understand the nature of our dataset, its limitations and the robustness of this result we performed a bootstrap resampling (with replacement) study of the 24 SNe II-P. In Figure 15 we present the results of this study for the variable α in Eq. 1 and the resultant rms. The rms peaks at 0.26 with a dispersion of 0.05 magnitudes and is well behaved. α peaks at 6.0 with a dispersion about the central peak of 0.5 (similar to that found in the formal χ^2 analysis), but shows a long tail to higher values potentially indicating the effect of small number statistics on this analysis.

4. Discussion

In this paper we have presented the first Hubble diagram for SNe II-P at cosmologically significant redshifts. The rms scatter of this method, 13% in distance, compares favorably to the 7-10% scatter seen in the SN Ia measurements (Riess et al. 1998; Perlmutter et al. 1999; Astier et al. 2005). This research has reached the stage of the early SNe Ia studies. Further improvements can now be sought with a view to reducing the scatter and increasing the cosmological power of the high-redshift data.

Examples of potential improvements include construction of new lightcurve templates to improve estimates of the explosion date. In Figure 10 the color of the SNLS-04D4fu, upon initial detection, implies temperatures of ∼20,000 K, suggesting this event was observed shortly after explosion and shock breakout, yet presently we do not incorporate this information to help constrain the explosion date. Furthermore, while we observed only 5 SNe II-P during the first two years of the SNLS program, the current photometric datasets contain many well observed lightcurves which, once redshifts have been obtained for the host galaxies, will allow us to place tight constraints on how various SNe II-P evolve as a function of time and thus better measure both their plateau colors and the date of explosion.

Additionally, dozens more nearby Hubble-flow SNe II-P have been observed by the CCCP and CSP both photometrically and spectroscopically. These data sets will allow us to better understand the velocity evolution of the spectroscopic features on the plateau and see if it is possible to use different photometric bands to standardize the SNe II-P while we improve our current methods. One question that this and future SNe II-P datasets must address is that of Malmquist bias. The two effects this can have on our analysis are a bias on the parameters we have determined in Eq. 1 and a bias on the discovery of lower luminosity events given the magnitude limited search. For the latter bias the important parameters to measure are the completeness limit of the search and the intrinsic dispersion on the corrected SNe II-P magnitudes (see Perlmutter et al. (1999) and references therein). From the data presented in this paper (see Figure 16) it is not clear whether or not Malmquist bias is a major issue or even which dataset, the low-redshift or high-redshift one, suffers from it more. Both the distributions in absolute magnitude and the velocity at day 50 are similar for each set.

Given multi-color lightcurves ($g'r'i'z'$) provided by SNLS, we conclude that this method *as-is* can be practically applied, using existing instrumentation, to $z = 0.3$. Over this redshift range we could detect the cosmic acceleration at >95% level, independent of any other constraints on the cosmological parameters, with $\simeq$12 additional high-redshift SNe II-P coupled with the five low-redshift CCCP SNe II-P observed this past year. Extending these measurements to $z = 0.5$ for the SNLS supernovae would require J-band imaging with *HST/NICMOS* for average luminosity SNe II-P. However, due to the wide dispersion in their apparent luminosity, a large fraction of this distribution could be observed in the infrared with 8-10 meter ground-based telescopes.

Exploring the utility of measuring distances to SNe II-P has potential benefits well beyond simply verifying, independently, the acceleration seen at redshifts z <1. Several plausible models for the time evolution of the dark energy require distance measures to $z \simeq$2 and beyond (Linder & Huterer 2003). At such high redshifts, other cosmological probes may become less effective than at $z \leq 1$. Weak lensing, for example, will suffer from the loss of suitable lenses, and, while evidence at $z < 1$ suggests some fraction of SNe Ia explode with very short delay-times and hence will be abundant at high-redshift (Mannucci et al. 2005; Sullivan et al. 2006), the efficiency and metallicity dependence of the SN Ia progenitor system is still in doubt and may curtail their production (e.g. Kobayashi et al. 1998). However, current models for the cosmic star-formation history predict an abundant source of SNe II at these epochs and future facilities, such as the proposed *JDEM* telescope, in concert with *JWST* and/or future 30-m telescopes such as TMT, could potentially use SNe II-P to determine distances at these very high redshifts.

Based on observations obtained with MegaPrime/MegaCam, a joint project of CFHT and CEA/DAPNIA, at the Canada-France-Hawaii Telescope (CFHT) which is operated by the National Research Council (NRC) of Canada, the Institut National des Science de l'Univers of the Centre National de la Recherche Scientifique (CNRS) of France, and the University of Hawaii. This work is based in part on data products produced at the Canadian Astronomy Data Centre as part of the Canada-France-Hawaii Telescope Legacy Survey, a collaborative project of NRC and CNRS. Some of the data presented herein were obtained at the W.M. Keck Observatory, which is operated as a scientific partnership among the California Institute of Technology, the University of California and the National Aeronautics and Space Administration. The Observatory was made possible by the generous financial support of the W.M. Keck Foundation. The authors wish to recognize and acknowledge the very significant cultural role and reverence that the summit of Mauna Kea has always had within the indigenous Hawaiian community. We are most fortunate to have the opportunity to conduct observations from this mountain. PEN acknowledges support from NASA ATP and LTSA grants. RSE acknowledges financial support from DOE. AG acknowledges support by NASA through Hubble Fellowship grant #HST-HF-01158.01-A awarded by STScI, which is operated by AURA, Inc., for NASA, under contract NAS 5-26555. DCL is supported by a National Science Foundation (NSF) Astronomy and Astrophysics Postdoctoral Fellowship under award AST-0401479. This research used resources of the National Energy Research Scientific Computing Center, which is supported by the Office of Science of the U.S. Department of Energy under Contract No. DE-AC03-76SF00098. We thank them for a generous allocation of computing time.

REFERENCES

Astier, P. et al. 2005, A&A, accepted

Baron, E., Nugent, P., Branch, D., Hauschildt, P. H., Leonard, D., Filippenko, A. V., Turatto, M., & Cappellaro, E. 2003, apj, 586, 1199

Baron, E., Nugent, P. E., Branch, D., & Hauschildt, P. H. 2004, ApJ, 616, 91

Benetti, S. 1991, in Supernova 1987A and other supernovae, ed. I. J. Danziger & K. Kjaaumlr (Garching, Germany: European Southern Observatory), 339

Bennett, C. L., Halpern, M., Hinshaw, G., Jarosik, N., Kogut, A., Limon, M., Meyer, S. S., Page, L., Spergel, D. N., Tucker, G. S., Wollack, E., Wright, E. L., Barnes, C., Greason, M. R., Hill, R. S., Komatsu, E., Nolta, M. R., Odegard, N., Peiris, H. V., Verde, L., & Weiland, J. L. 2003, ApJS, 148, 1

Cappellaro, E., Riello, M., Altavilla, G., Botticella, M. T., Benetti, S., Clocchiatti, A., Danziger, J. I., Mazzali, P., Pastorello, A., Patat, F., Salvo, M., Turatto, M., & Valenti, S. 2005, A&A, 430, 83

Chugai, N. N. 1994, in Circumstellar Media in Late Stages of Stellar Evolution, 148–+

Efstathiou, G., Moody, S., Peacock, J. A., Percival, W. J., Baugh, C., Bland-Hawthorn, J., Bridges, T., Cannon, R., Cole, S., Colless, M., Collins, C., Couch, W., Dalton, G., de Propris, R., Driver, S. P., Ellis, R. S., Frenk, C. S., Glazebrook, K., Jackson, C., Lahav, O., Lewis, I., Lumsden, S., Maddox, S., Norberg, P., Peterson, B. A., Sutherland, W., & Taylor, K. 2002, MNRAS, 330, L29

Eisenstein, D. J., Blanton, M., Zehavi, I., Bahcall, N., Brinkmann, J., Loveday, J., Meiksin, A., & Schneider, D. 2005, ApJ, 619, 178

Ellis, R. S. et al. 2006, in preparation

Forster, F. et al. 2006, MNRAS, submitted

Freedman, W. L. . T. C. S. P. 2005, in ASP Conf. Ser. 339: Observing Dark Energy, 50–+

Gal-Yam, A., Cenko, S. B., Fox, D. W., Leonard, D. C., Moon, D.-S., Sand, D. J., & Soderberg, A. M. 2004, American Astronomical Society Meeting Abstracts, 205,

Gal-Yam, A. et al. 2006a, in preparation

—. 2006b, apj, in preparation

Guy, J., Astier, P., Nobili, S., Regnault, N., & Pain, R. 2005, A&A, 443, 781

Hamuy, M. 2002, PhD thesis, University of Arizona

Hamuy, M. 2003, in I.A.U. Colloquium 192: Supernovae (10 years of SN1993J), ed. J. Marcaide & K. Weiler (Valencia, Spain: Springer Verlag)

Hamuy, M. & Pinto, P. A. 2002, ApJ, 566, 63

Hamuy, M., Pinto, P. A., Maza, J., Suntzeff, N. B., Phillips, M. M., Eastman, R. G., Smith, R. C., Corbally, C. J., Burstein, D., Li, Y., Ivanov, V., Moro-Martin, A., Strolger, L. G., de Souza, R. E., dos Anjos, S., Green, E. M., Pickering, T. E., González, L., Antezana, R., Wischnjewsky, M., Galaz, G., Roth, M., Persson, S. E., & Schommer, R. A. 2001, apj, 558, 615

Heger, A., Fryer, C. L., Woosley, S. E., Langer, N., & Hartmann, D. H. 2003, ApJ, 591, 288

Kirshner, R. P. & Kwan, J. 1974, apj, 193, 27

Knop, R. A. et al. 2003, apj, 598, 102

Kobayashi, C., Tsujimoto, T., Nomoto, K., Hachisu, I., & Kato, M. 1998, ApJ, 503, L155

Leonard, D. C. 2000, PhD thesis, University of California, Berkeley

Leonard, D. C. & Filippenko, A. V. 2005, in 1604-2004: Supernovae as Cosmological Lighthouses, ed. S. B. M. Turatto, W. R. J. Shea & L. Zampieri (Padua, Italy: ASP), 100

Leonard, D. C., Filippenko, A. V., Li, W., Matheson, T., Kirshner, R. P., Chornock, R., Van Dyk, S. D., Berlind, P., Calkins, M. L., Challis, P. M., Garnavich, P. M., Jha, S., & Mahdavi, A. 2002, AJ, 124, 2490

Leonard, D. C., Kanbur, S. M., Ngeow, C. C., & Tanvir, N. R. 2003, ApJ, 594, 247

Li, W., Van Dyk, S. D., Filippenko, A. V., & Cuillandre, J.-C. 2005, PASP, 117, 121

Linder, E. V. & Huterer, D. 2003, Phys. Rev. D, 67, 081303

Mannucci, F., della Valle, M., Panagia, N., Cappellaro, E., Cresci, G., Maiolino, R., Petrosian, A., & Turatto, M. 2005, A&A, 433, 807

Mitchell, R. et al. 2002, apj, 574

Moore, M. & Li, W. 2004, IAU Circ. No. 8375

Nugent, P., Kim, A., & Perlmutter, S. 2002, PASP, 114, 803

Oke, J. B., Cohen, J. G., Carr, M., Cromer, J., Dingizian, A., Harris, F. H., Labrecque, S., Lucinio, R., Schaal, W., Epps, H., & Miller, J. 1995, PASP, 107, 375

Perlmutter, S. et al. 1999, apj, 517, 565

Riess, A. et al. 1998, AJ, 116, 1009

Schmidt, B. P. 1993, PhD thesis, Harvard University

Smartt, S. J., Maund, J. R., Gilmore, G. F., Tout, C. A., Kilkenny, D., & Benetti, S. 2003, MNRAS, 343, 735

Strolger, L., Riess, A. G., Dahlen, T., Livio, M., Panagia, N., Challis, P., Tonry, J. L., Filippenko, A. V., Chornock, R., Ferguson, H., Koekemoer, A., Mobasher, B., Dickinson, M., Giavalisco, M., Casertano, S., Hook, R., Blondin, S., Leibundgut, B., Nonino, M., Rosati, P., Spinrad, H., Steidel, C. C., Stern, D., Garnavich, P. M., Matheson, T., Grogin, N., Hornschemeier, A., Kretchmer, C., Laidler, V. G., Lee, K., Lucas, R., de Mello, D., Moustakas, L. A., Ravindranath, S., Richardson, M., & Taylor, E. 2004, ApJ, 613, 200

Sullivan, M. et al. 2005, in 1604-2004: Supernovae as Cosmological Lighthouses, ed. S. B. M. Turatto, W. R. J. Shea & L. Zampieri (Padua, Italy: ASP), 1

Sullivan, M. et al. 2006, in preparation

Tonry, J. & Davis, M. 1979, AJ, 84, 1511

Tonry, J. L., Blakeslee, J. P., Ajhar, E. A., & Dressler, A. 2000, ApJ, 530, 625

Turatto, M., Cappellaro, E., Benetti, S., & Danziger, I. J. 1993, MNRAS, 265, 471

Table 1. Cross-Correlation Velocity Analysis for $H\beta$ Dominated Spectra

SNLS Name	Template Spectrum (Epoch)	$H\beta$ Velocity (km/s)	$H\beta$/Fe II Ratio	Fe II Velocity (km/s)
03D3ce	SN 1999em (15)	8137.6 ± 42.0	1.256 ± 0.054	6479.0 ± 350
03D4cw	SN 2004T (15)	7355.4 ± 56.3	1.307 ± 0.054	5627.7 ± 304

Note. — The best match nearby template spectrum from our library along with the the resultant median absolute deviation velocity measurement, with a 3 median-absolute-deviations cut, for the $H\beta$ dominated SNLS supernovae. Also listed are the $H\beta$ to Fe II ratios and the resultant Fe II velocities. Approximate epochs for the nearby SNe II-P are in parens.

Table 2. Cross-Correlation Velocity Analysis for Fe II Dominated Spectra

SNLS Name	Template Spectrum (Epoch)	Fe II Velocity (km/s)
04D1ln	SN 1999em (61)	3201.8 ± 86.9
04D1pj	SN 2004em (35)	5478.5 ± 72.5
04D4fu	SN 2004A (50)	3280.5 ± 35.1

Note. — The best match nearby template spectrum from our library along with the the resultant median absolute deviation velocity measurement, with a 3 median-absolute-deviations cut, for the Fe II dominated SNLS supernovae. Approximate epochs for the nearby SNe II-P are in parens.

Table 3. Measurements for the SNLS high-redshift SNe II-P

SNLS Name	z	t_{expl}	t_{spec}	$V_{Fe\ II}$ (km/s)	I	$V-I$	μ
03D3ce	0.2881	2771.5 ± 12.0	2821.9	5762 ± 522	23.45 ± 0.50	0.39 ± 0.50	41.10 ± 0.40
03D4cw	0.1543	2863.0 ± 10.5	2878.9	3067 ± 660	22.33 ± 0.09	0.90 ± 0.10	39.11 ± 0.55
04D1ln	0.2077	3276.5 ± 6.0	3353.9	3593 ± 159	22.79 ± 0.05	0.70 ± 0.07	39.70 ± 0.15
04D1pj	0.1556	3305.8 ± 5.5	3352.9	4981 ± 214	21.99 ± 0.04	0.66 ± 0.06	39.69 ± 0.15
04D4fu	0.1330	3217.5 ± 7.0	3297.9	3861 ± 150	21.99 ± 0.04	0.59 ± 0.05	38.94 ± 0.14

Note. — All dates are in the observer-frame and are expressed as (JD-2450000) and the uncertainties in the explosion date are not corrected for time dilation. The magnitudes have been corrected for MW extinction along the line of sight. The large uncertainties for SNLS-03D3ce are due to the fact that it was not observed in z', which at its redshift overlaps with restframe I-band. For this supernova we derived it's $V-I$ color by finding the best match in our template day 50 spectra to its observed $g'r'i'$ magnitudes. We then set the dispersion in the $V-I$ color to 50%, which covers the range of all uncorrected colors for the SNe II-P presented in this paper. Our Monte Carlo (see text) was used to derive both the peak values and the uncertainties in the distance modulii. In general, the major contribution to the uncertainty in the distance are (in decreasing significance): explosion date uncertainty, length of extrapolation to day 50, velocity uncertainty and photometry.

Table 4. Measurements for the Local & Hubble-Flow SNe II-P

IAUC Name	cz	$V_{Fe\ II}$ (km/s)	I	$V-I$	μ
1986I	1333	3623 ±300	13.98 ± 0.09	0.45 ± 0.22	30.58 ± 0.43
1989L	1332	3529 ±300	14.47 ± 0.05	0.88 ± 0.07	31.60 ± 0.38
1990E	1426	5324 ±300	14.51 ± 0.20	1.31 ± 0.28	33.24 ± 0.43
1990K	1818	6142 ±2000	13.87 ± 0.05	0.58 ± 0.21	31.96 ± 0.87
1991al	4484	7330 ±2000	16.06 ± 0.05	0.39 ± 0.07	34.33 ± 0.70
1991G	1152	3347 ±500	15.01 ± 0.09	0.45 ± 0.11	31.43 ± 0.53
1992af	5438	5322 ±2000	16.46 ± 0.20	0.43 ± 0.28	33.99 ± 0.99
1992am	14009	7868 ±300	17.90 ± 0.05	0.38 ± 0.07	36.33 ± 0.12
1992ba	1192	3523 ±300	14.65 ± 0.05	0.59 ± 0.07	31.38 ± 0.41
1993A	8933	4290 ±300	18.56 ± 0.05	0.51 ± 0.07	35.67 ± 0.20
1993S	9649	4569 ±300	18.22 ± 0.05	0.69 ± 0.07	35.73 ± 0.18
1999br	848	1545 ±300	16.67 ± 0.05	0.84 ± 0.07	31.70 ± 0.69
1999ca	3105	5353 ±2000	15.56 ± 0.05	0.73 ± 0.07	33.51 ± 0.95
1999cr	6376	4389 ±300	17.44 ± 0.05	0.56 ± 0.07	34.68 ± 0.20
1999eg	6494	4012 ±300	17.72 ± 0.05	0.55 ± 0.07	34.71 ± 0.21
1999em	917	3757 ±300	13.28 ± 0.05	0.57 ± 0.07	30.15 ± 0.49
1999gi	901	3617 ±300	13.95 ± 0.05	0.91 ± 0.07	31.18 ± 0.50
2000cb	2038	4732 ±300	15.48 ± 0.05	0.71 ± 0.07	33.10 ± 0.26
2004dh	5778	4990 ±300	17.32 ± 0.05	0.47 ± 0.07	34.74 ± 0.18

Note. — Data from Hamuy & Pinto (2002); Hamuy (2003) with modifications to SNe 1999em and 1999gi as stated in the text. SN 2004dh is from preliminary work by the CCCP (Gal-Yam et al. 2004; Gal-Yam et al. 2006a). All magnitudes have been corrected for MW extinction along the line of sight.

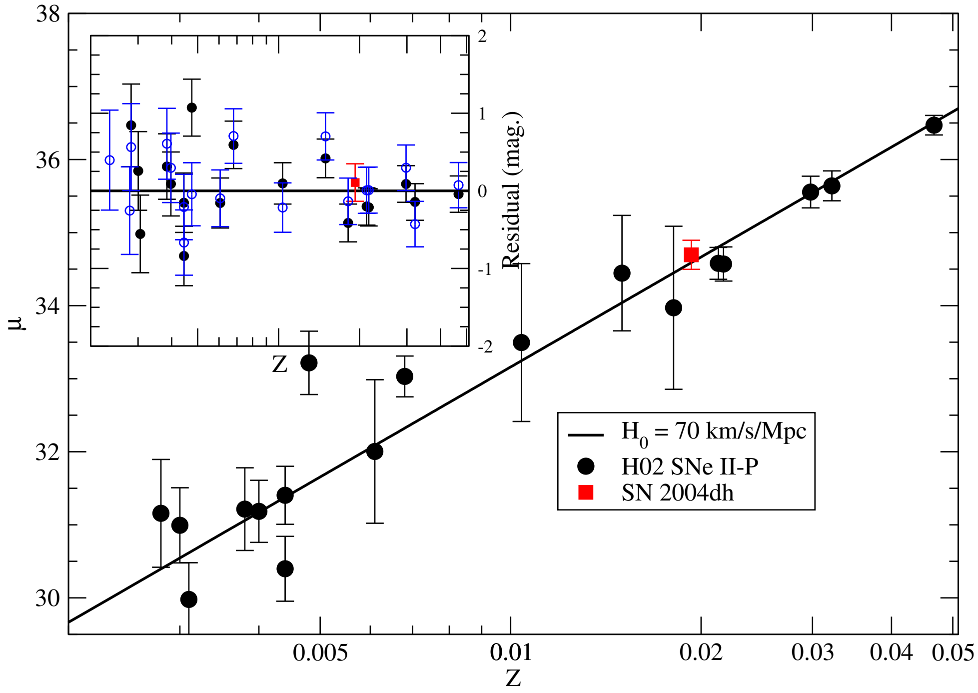

Fig. 1.— A revised Hubble diagram (scaled to $H_0 = 70$ km/s/Mpc) for local SNe II-P (diamonds and square) using an improved estimator for extinction derived from $V-I$ colors and Fe II velocities observed during the plateau phase at day 50. *Inset:* The residual Hubble diagram for both the revised method (black) and the data under the assumption that they are pure standard candles in I-band, corrected only for MW extinction (blue). The scatter for those SN II-P in the Hubble flow is reduced from 0.59 to 0.28 magnitudes, similar to the 0.29 magnitudes originally achieved in H03 and based on observables substantially better suited to high-redshift observations. The scatter for all SN II-P is reduced from 1.11 to 0.52 magnitudes.

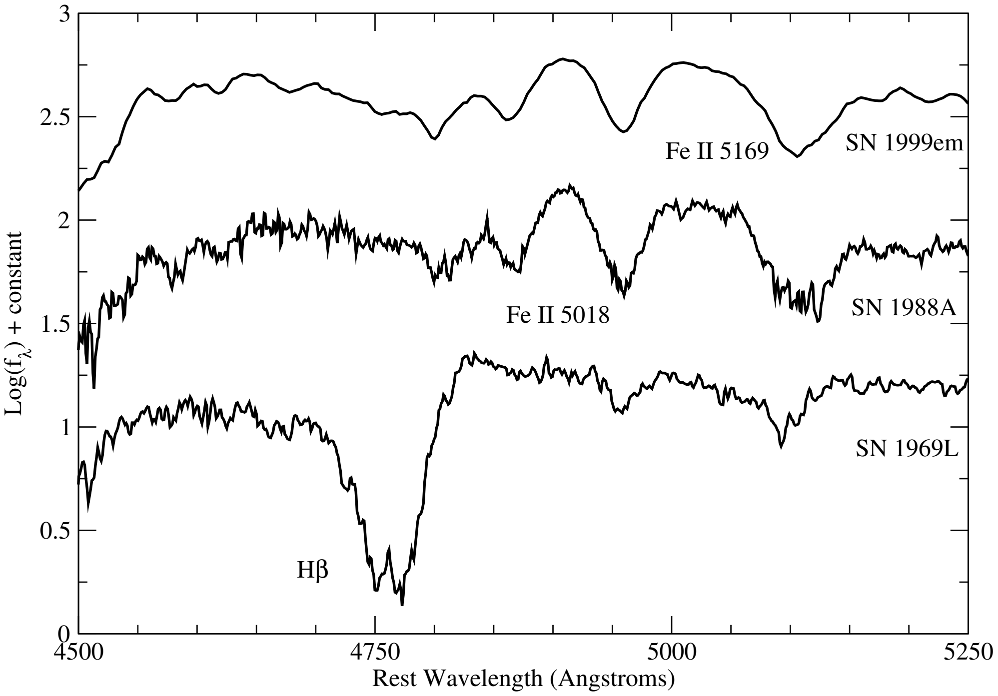

Fig. 2.— A comparison of two Fe II-dominated spectra to an $H\beta$-dominated spectrum. This demarcation is defined by the equivalent width of $H\beta$ being greater than the sum of the Fe II features. Depending on the supernova and its phase, any one of these features could potentially be the strongest and/or the most easily measured (due to sky lines or host galaxy contamination) and thus could be used at high redshift.

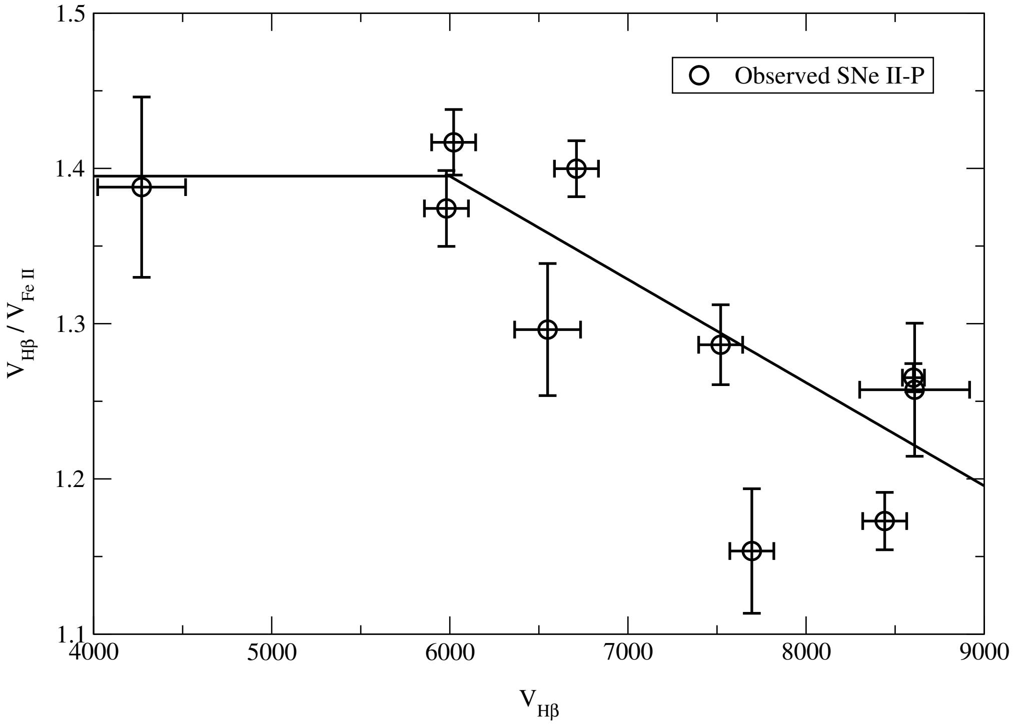

Fig. 3.— The ratio of the velocities of $H\beta$ to Fe II 5169Å vs. the $H\beta$ velocity in the $H\beta$-dominated spectra. We fit this ratio in two pieces, a constant for velocities below 6000 km/s ($ratio = 1.395$) and linearly for higher velocities ($ratio = 1.395 - 6.489 * 10^{-5}(V(H\beta) - 6000)$). The linear portion is the only one relevant to our analysis as our high-redshift data lie within these velocities. The dispersion about this relationship (± 0.054) translates to an uncertainty in measuring the Fe II velocity from $H\beta$ of $\sim$300 km/s. See text for a full discussion and explanation of this trend.

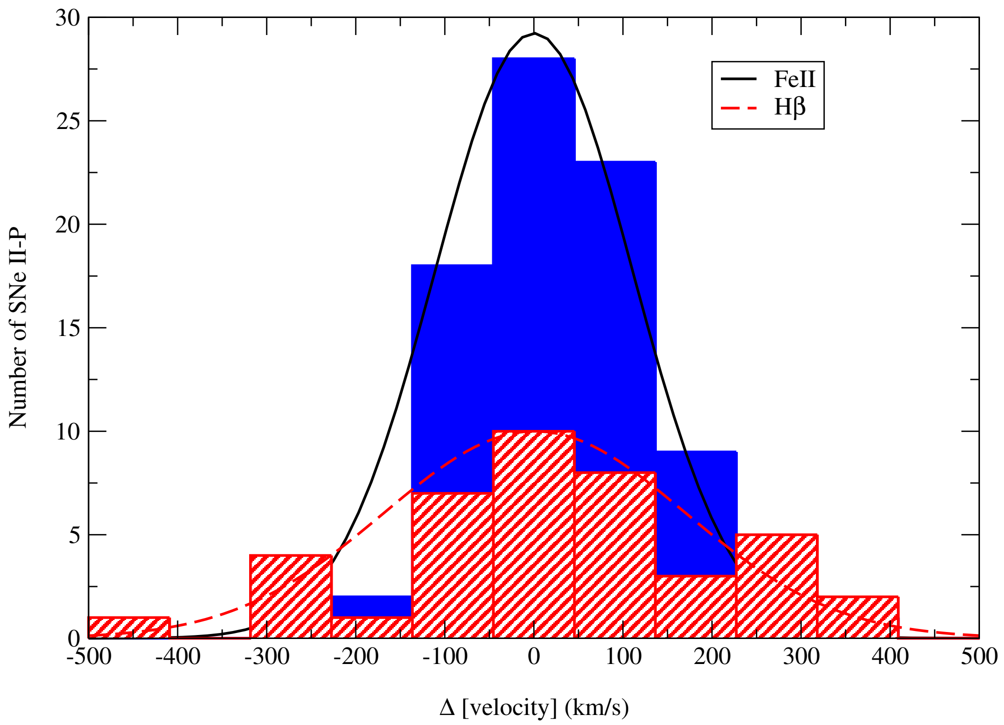

Fig. 4.— A histogram of the difference in measured velocity vs. the velocity derived from the cross-correlation technique for Fe II 5169Å and $H\beta$. Here we have compared each SN II-P in our library to all the others, splitting the comparison library for SN II-P to those that are dominated by $H\beta$ and those by Fe II. The measured dispersion is 161 km/s for the $H\beta$ subset and 108 km/s for the Fe II subset.

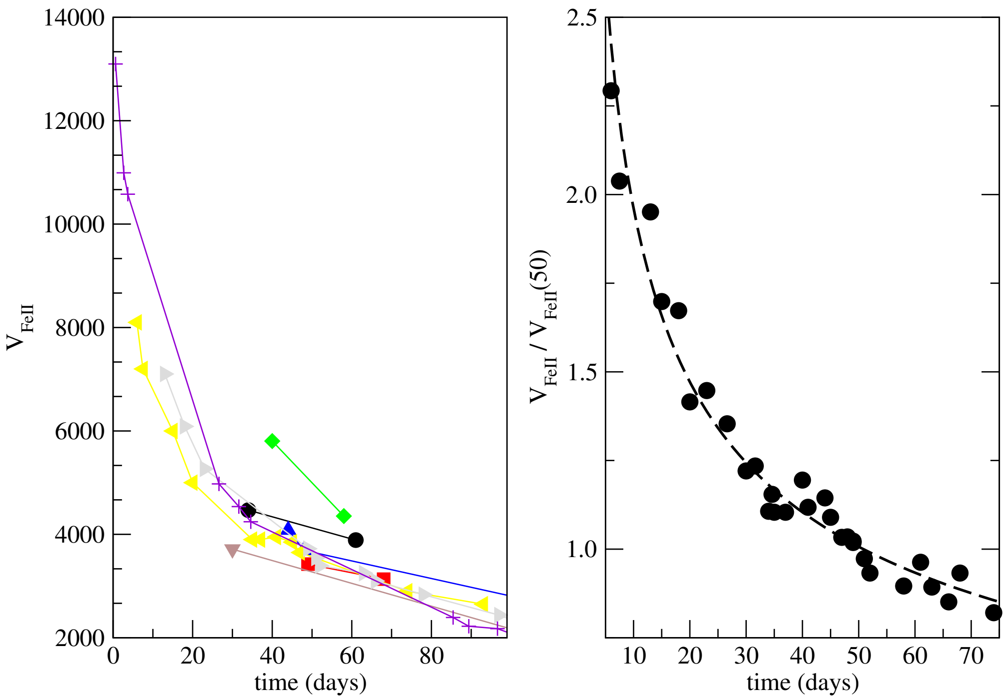

Fig. 5.— *Left:* A plot of the velocity of Fe II 5169Å vs. time for the published SNe II-P (each symbol represents an individual supernova). *Right:* A plot of the individual SNe II-P with their velocities normalized to day 50, along with the best fit for the evolution of the decline covering the epochs for our high-redshift supernovae (day 9–75). The fit is a power law of the form $V(50) = V(t) * (t/50)^{0.464 \pm 0.017}$.

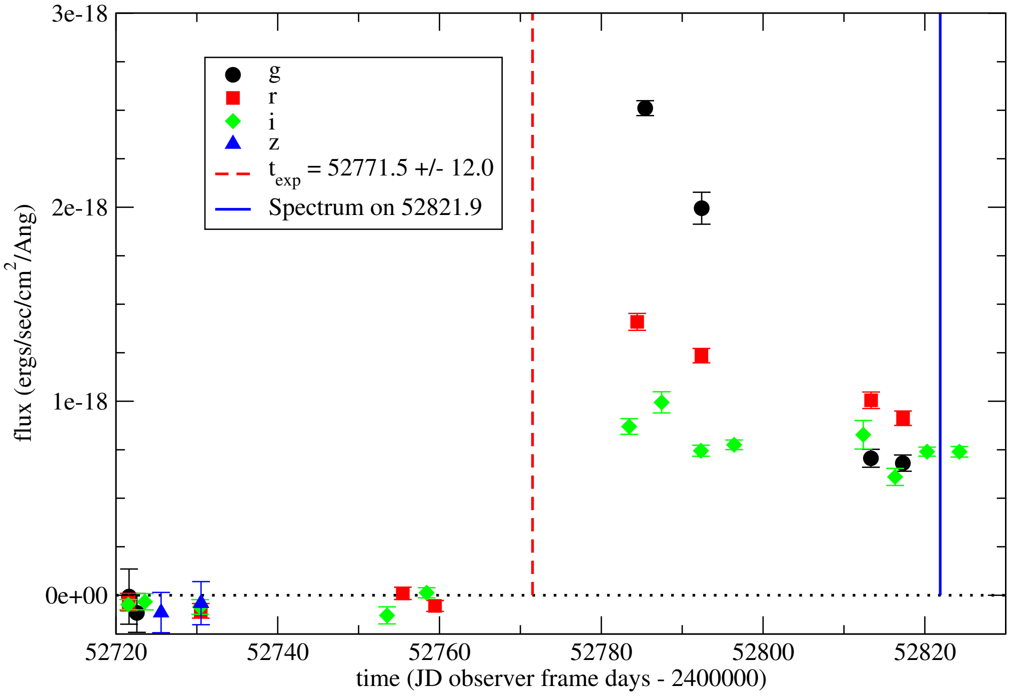

Fig. 6.— The SNLS $g'r'i'z'$ lightcurves (in f_λ) for SNLS-03D3ce at a $z = 0.2881$. Unfortunately this SN was not observed in z' on the plateau. At this redshift z' overlaps nicely with restframe I-band, thus the $V - I$ color had to be extrapolated from bluer colors than desired for this SN II-P.

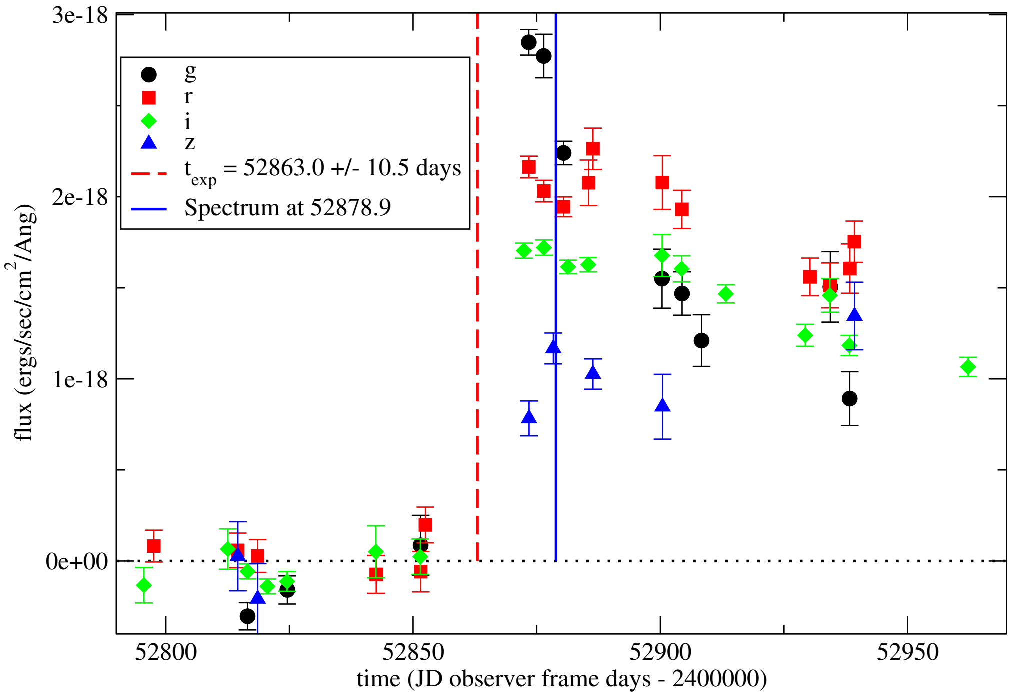

Fig. 7.— The SNLS $g'r'i'z'$ lightcurves (in f_λ) for SNLS-03D4cw at a $z = 0.1543$.

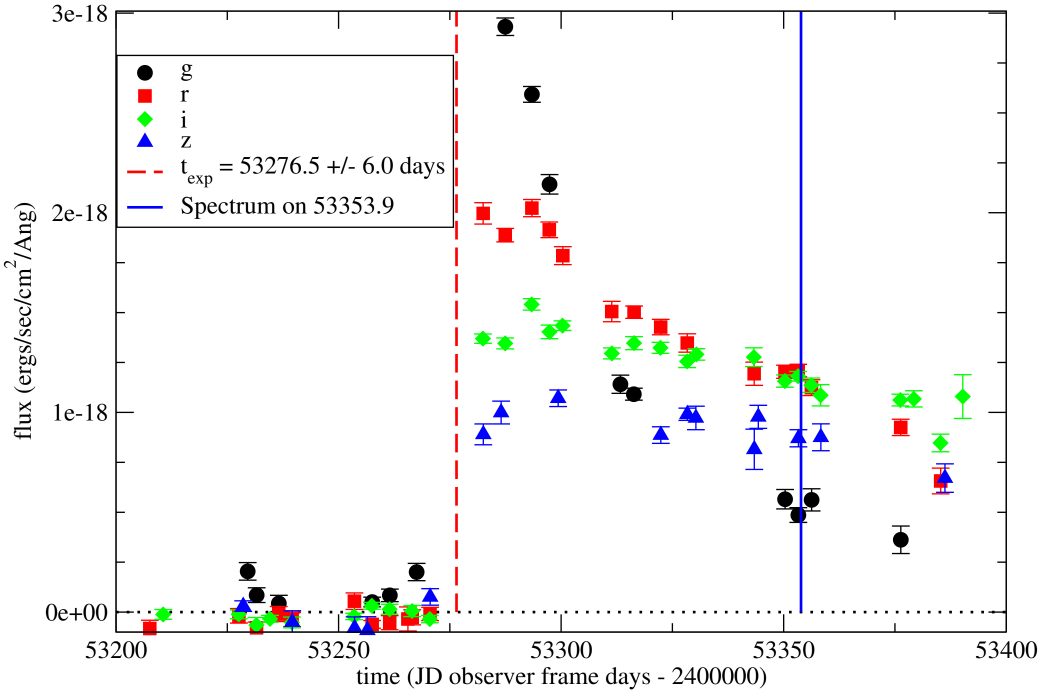

Fig. 8.— The SNLS $g'r'i'z'$ lightcurves (in f_λ) for SNLS-04D1ln at a $z = 0.2078$.

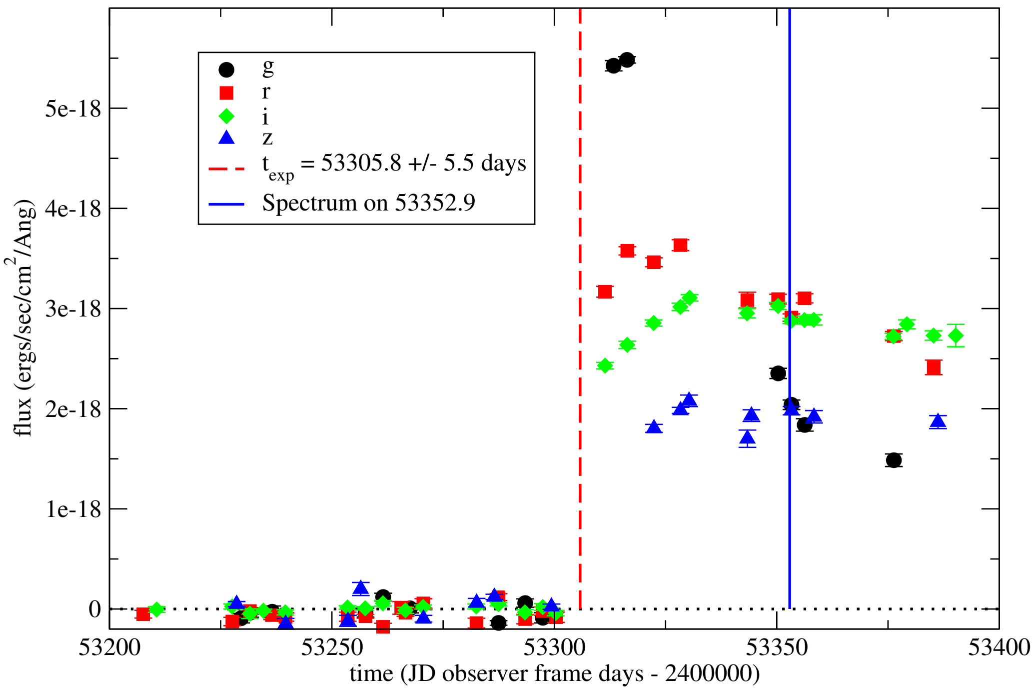

Fig. 9.— The SNLS $g'r'i'z'$ lightcurves (in f_λ) for SNLS-04D1pj at a $z = 0.1556$.

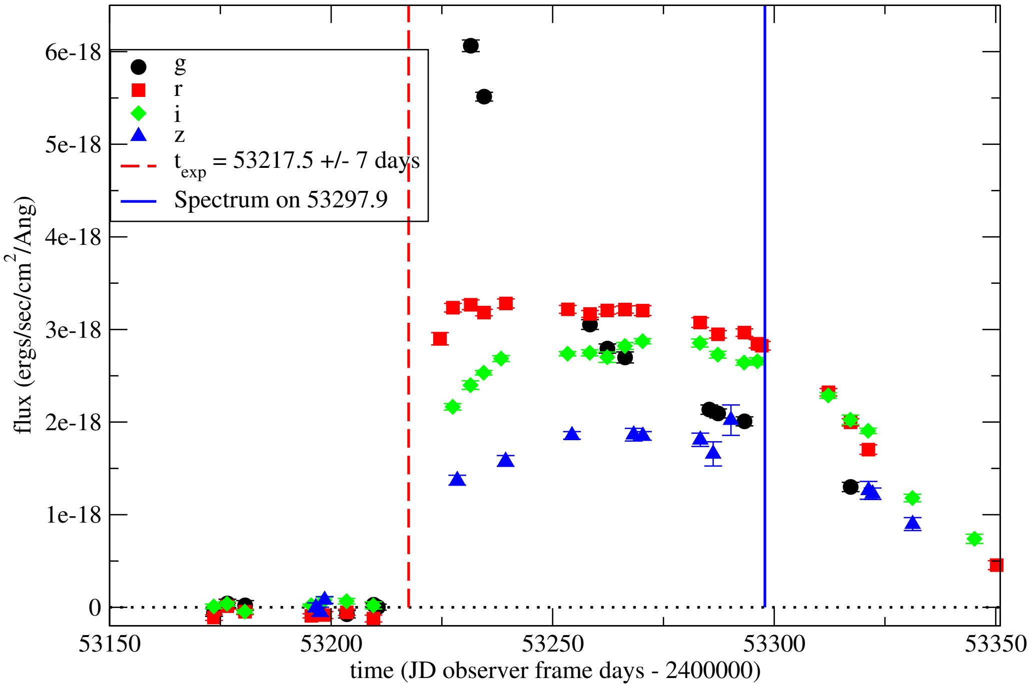

Fig. 10.— The SNLS $g'r'i'z'$ lightcurves (in f_λ) for SNLS-04D4fu at a $z = 0.1330$. This supernova was caught just after shock-breakout as the $g'r'i'z'$ colors (uncorrected for extinction) lead to a temperature $>$ than 20,000 K.

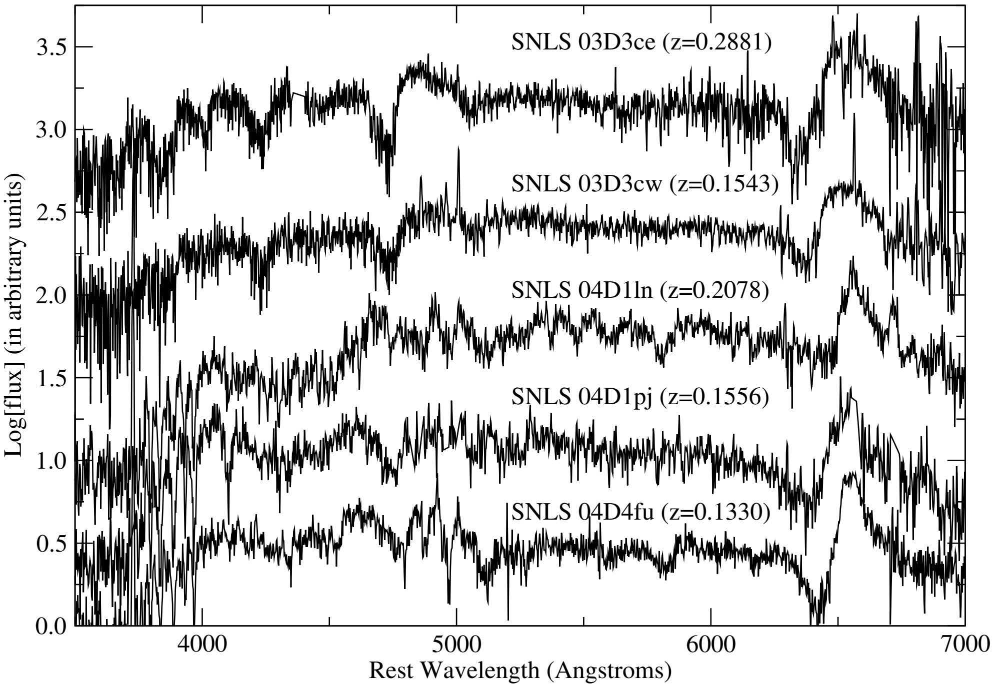

Fig. 11.— The restframe spectra of the high-redshift SNe II-P observed at Keck+LRIS in 2003 and 2004. From top to bottom they are: SNLS 03D3ce, 03D4cw, 04D1ln, 04D1pj and 04D4fu. The quality of these spectra is such that the measurement of the Fe II velocities, based on the technique described in § 2.2 over the range 4500-5500 Å, is good to ∼250 km/s.

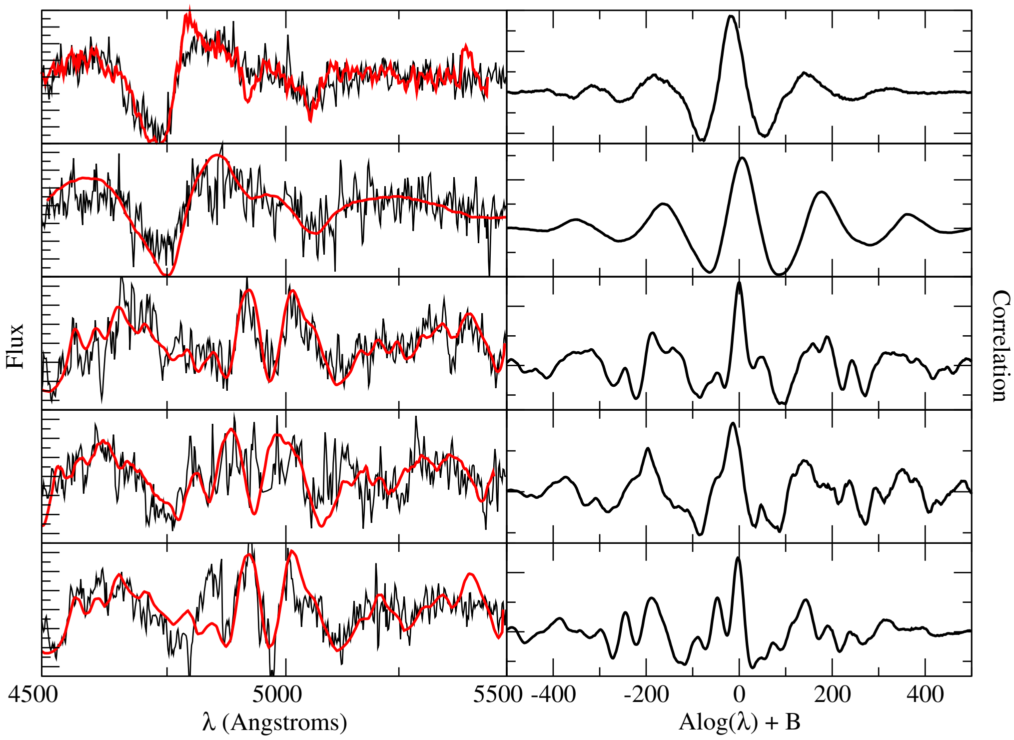

Fig. 12.— *Left-hand-side*: A plot of the best fit template spectrum (thick line) and the SNLS SNe II-P (thin line) used in the cross-correlation technique. *Right-hand-side*: The resultant correlation. Plotted from top to bottom are: SNLS-03D3ce, 03D4cw, 04D1ln, 04D1pj and 04D4fu.

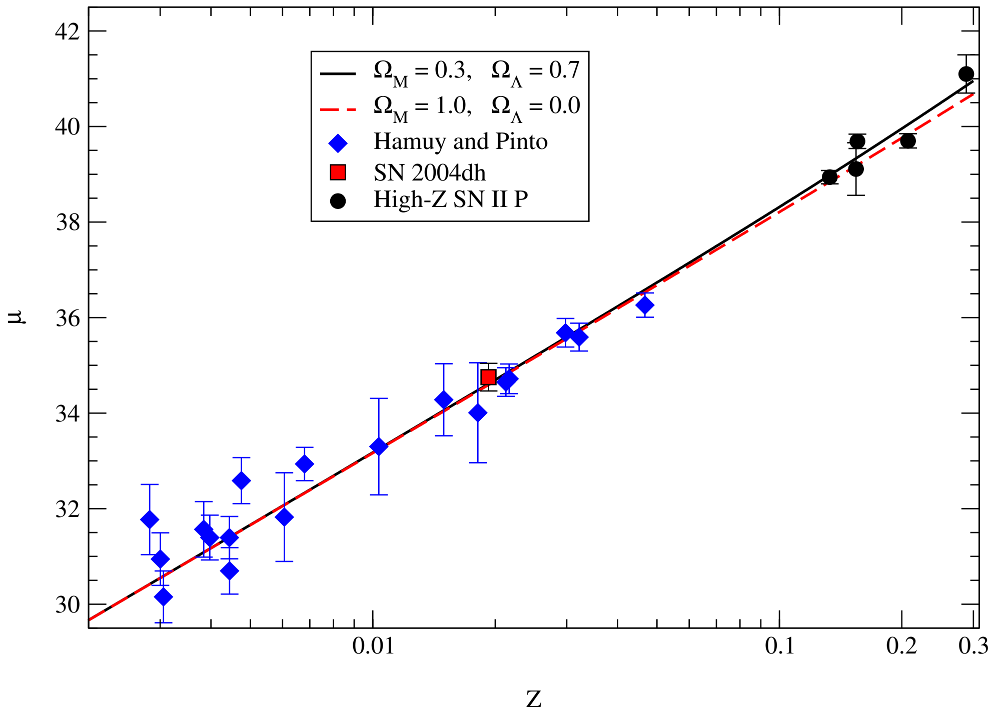

Fig. 13.— The Hubble diagram for both the local SNe II-P (diamonds and square) and the high-redshift SNLS SNe II-P (circles) observed spectroscopically with Keck+LRIS. The observed scatter for the supernova in the Hubble flow is 0.26 magnitudes with a reduced χ^2 of 1.8, which is indicates an intrinsic dispersion of 0.12 magnitudes. To understand the current power of this technique we have over-plotted two differing Hubble lines for a flat cosmology with $\Omega_M = 1$ and 0.3.

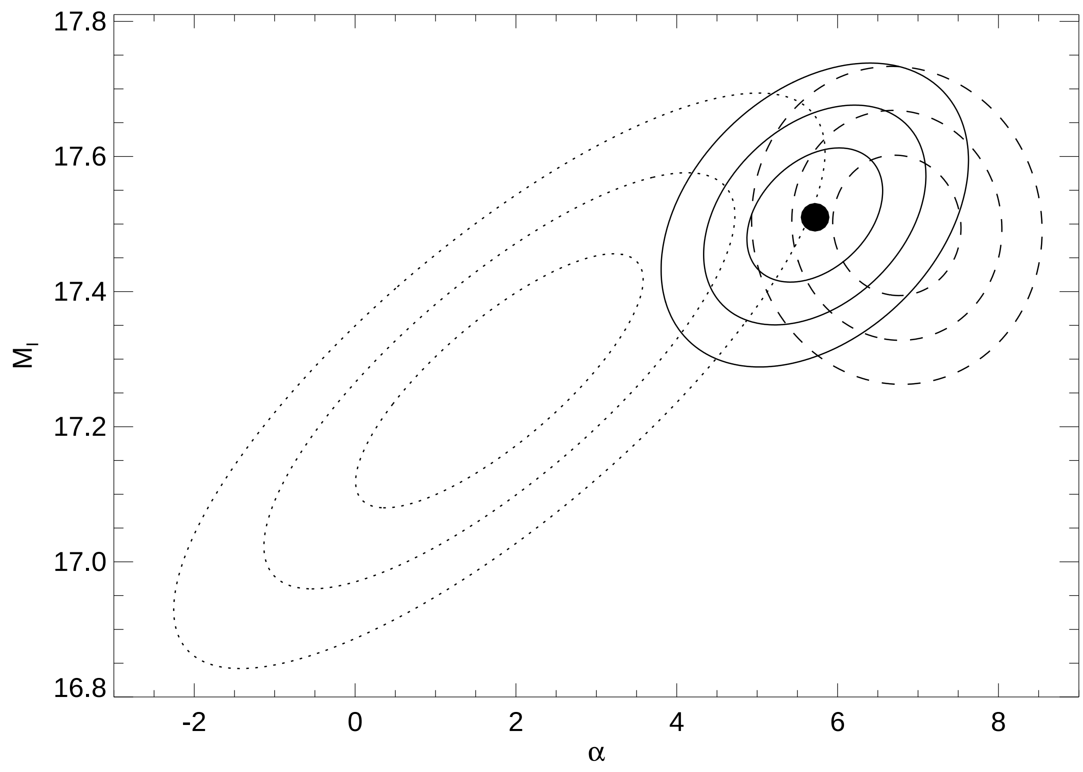

Fig. 14.— The 1, 2 and 3-σ confidence contours in the α–M_{I_0} plane for the low-redshift only (dashed), high-redshift only (dotted) and combined SNe II-P data sets (solid). Due to low-number statistics at both high and low-redshift these parameters are still poorly determined for precision cosmology. Future research by the CCCP and CSP will improve our understanding of this relationship considerably.

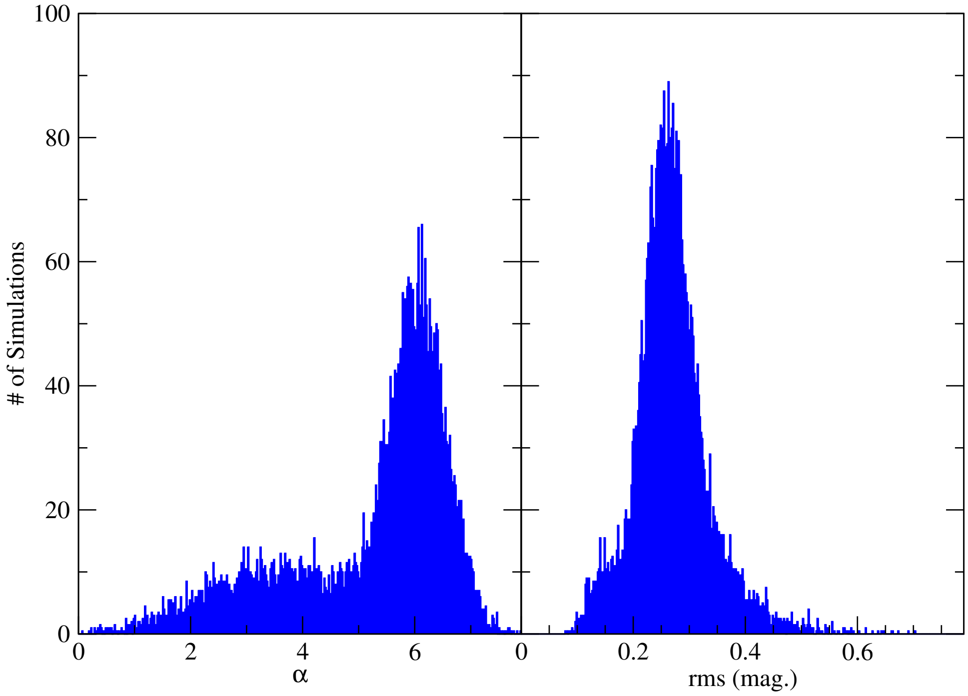

Fig. 15.— A bootstrap resampling (with replacement) study of the variable α and the rms of the 24 SNe II-P presented in this paper. While the rms is nicely behaved, α indicates that our dataset may be susceptible to small number statistics.

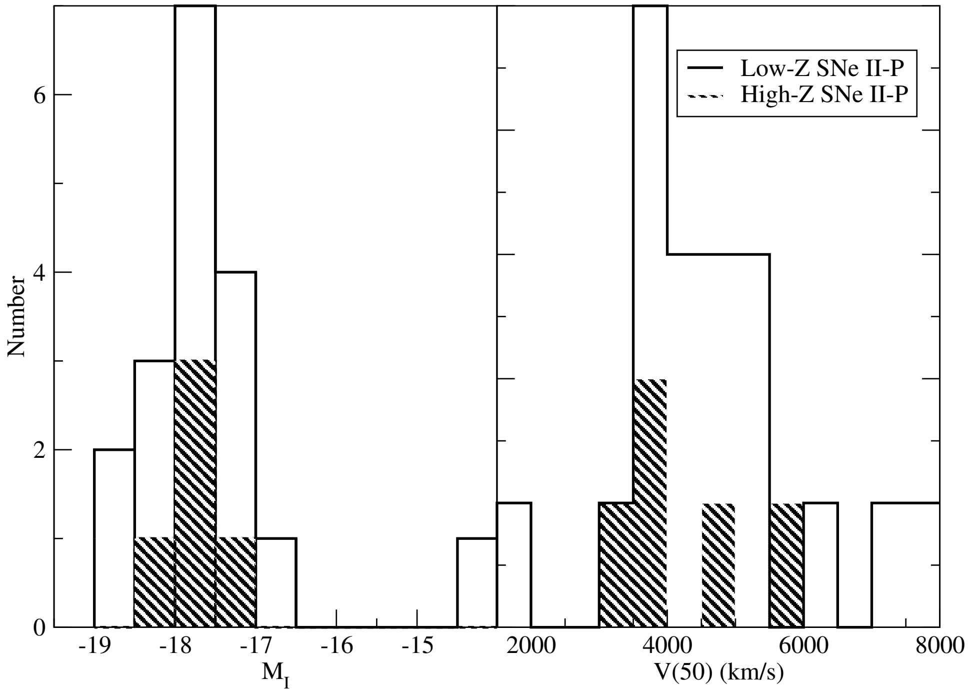

Fig. 16.— Histograms of the observed absolute magnitude in I-band, uncorrected for extinction, and the day 50 velocities, for both the high-redshift (filled) and low-redshift (open) SNe II-P. Future datasets will have to address the important issue of Malmquist bias, a question beyond the scope of this paper.